Steady-State Hollow Electron Temperature Profiles in the Rijnhuizen Tokamak Project

G. M. D. Hogeweij, A. A. M. Oomens, C. J. Barth, M. N. A. Beurskens, C. C. Chu, J. F. M. van Gelder, J. Lok, N. J. Lopes Cardozo, F. J. Pijper, R. W. Polman, and J. H. Rommers
FOM Instituut voor Plasmafysica "Rijnhuizen," Associatie EURATOM-FOM, P.O.Box 1207, 3430 BE Nieuwegein, The Netherlands
(Received 6 October 1995)

In the Rijnhuizen Tokamak Project steady-state hollow electron temperature (T_e) profiles have been sustained with strong off-axis electron cyclotron heating, creating a region of reversed magnetic shear. In this region the effective electron thermal diffusivity (χ_e^{pb}) is close to neoclassical in high density plasmas. For medium density, χ_e^{pb} is lower than neoclassical and may even be negative, indicating that off-diagonal elements in the transport matrix drive an electron heat flux up the T_e gradient.

PACS numbers: 52.55.Fa, 52.25.Fi, 52.50.Gj

The transport of energy and particles across the magnetic field in a magnetized plasma is a largely unexplained phenomenon. In a tokamak, the leading candidate for a fusion reactor based on magnetic confinement, the transport problem is in first order one dimensional, due to its toroidal geometry of nested flux surfaces. All physical parameters are one-dimensional functions (often called profiles) of the normalized minor radius ρ.

A common observation in tokamak plasmas is that the electron and ion temperature profiles $T_e(\rho)$ and $T_i(\rho)$ always have roughly the same shape, regardless of the method and localization of the heating [1–5]. This phenomenon is usually called profile resilience; various theoretical models have been developed to explain it [6–9]. The most pronounced example of profile resilience is the peaking of the T_e profile which was found in medium density DIII-D plasmas even when strong electron cyclotron heating (ECH) was applied with off-axis absorption [10].

This Letter presents recent experimental results, showing that profile resilience can be broken by strong off-axis ECH in a medium to high density plasma. Steady-state hollow T_e profiles have been obtained for a wide range of the electron density n_e and power deposition radius ρ_{dep}. In these cases a region of negative magnetic shear exists inside ρ_{dep} after full current adaptation.

The experiments were carried out at the Rijnhuizen Tokamak Project (RTP). This machine (major radius $R_0 = 0.72$ m, minor radius $a = 0.164$ m, toroidal magnetic field $B_T \le 2.4$ T, plasma current $I_p \le 150$ kA, pulse duration $\le$600 ms) is equipped with an ECH system [11], comprising of, amongst others, a 110 GHz, 500 kW, 200 ms gyrotron, injecting from the low field side (LFS) in second harmonic *X* mode. Crucial for the experiments reported here is the Thomson scattering (TS) system, measuring T_e and n_e along a vertical chord through the center of the plasma at ~110 radial positions simultaneously, with a spatial resolution of 2.5 mm [12,13].

In a series of off-axis heating experiments with the 110 GHz gyrotron, 350–400 kW was injected into ohmic target plasmas [hydrogen, $I_p = 80$–120 kA, $B_T = 1.7$–2.4 T, edge safety factor $q_a = 3.3$–5.5, central electron density $n_e(0) = (2 - 8) \times 10^{19}$ m^{-3}, and effective ion charge $Z_{\text{eff}} \simeq 1.5$–$2.5$]. The power was deposited either on the LFS or on the high field side (HFS), at $\rho_{\text{dep}} = 0.3$–0.6. Profiles of T_e and n_e were taken 80 ms after the switch-on of ECH, i.e., when a steady state has been reached, taking current diffusion into account.

In low plasma current plasmas ($I_p = 80$ kA, i.e., $q_a = 4.0$–5.5), the following observations were made. At low density off-axis ECH creates flat T_e profiles inside ρ_{dep}. Above a threshold central density $n_e(0)_{\text{thresh}} \simeq 3.5 \times 10^{19}$ m^{-3}, off-axis ECH creates steady-state hollow T_e profiles. The central hole in $T_e(\rho)$ is attributed to the heat transfer from electrons to ions (p_{e-i}), which increases with increasing n_e. These observations were made for both HFS and LFS absorption. Figure 1 shows the different effects of on- and off-axis heating. Figure 2 shows the transition from flat to hollow T_e with increasing density. Figure 3 shows T_e profiles for different ρ_{dep}. The n_e profile modifies slightly during off-axis heating. The electron pressure (p_e) profile

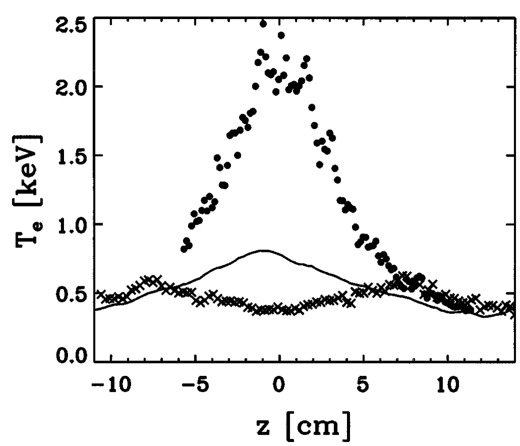

FIG. 1. T_e profiles of a centrally heated (•) and an off-axis heated (×) RTP discharge. For comparison the profile of a similar Ohmic discharge is plotted (full line). For these discharges $I_p = 80$ kA and $n_e(0) = 4.0 \times 10^{19}$ m^{-3}.

 0031-9007/96/76(4)/632(4)$06.00

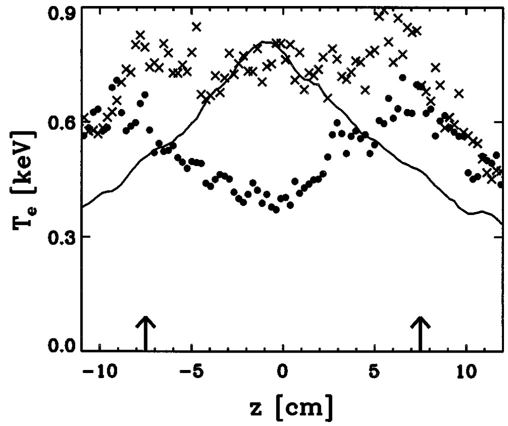

FIG. 2. T_e profiles with off-axis ECH, for $n_e(0) = 3.0 \times 10^{19}$ (×) and 4.0×10^{19} m^{-3} (•), showing the transition from flat to hollow T_e with increasing density (RTP discharges r19950620.008 and r19950620.019, respectively). The arrow marks ρ_{dep}. For comparison the profile of a similar ohmic discharge is plotted (full line).

flattens strongly, and can be completely flat out to ρ_{dep} under these conditions. Figure 4 shows T_e, n_e, and p_e profiles for different ρ_{dep}. The TS profiles are confirmed by electron cyclotron emission (ECE) measurements, showing cooling in the center after the switch-on of ECH at a time scale of $\simeq$20 ms (Fig. 5), consistent with the calculated current diffusion time. First polarimetry measurements confirmed that the current density profile (j) adapts on this time scale [14].

At higher I_p, off-axis ECH causes a flattening of T_e out to ρ_{dep}, but no hollow T_e profiles have been observed. This is attributed to the stronger residual central Ohmic heating at high I_p, which compensates p_{e-i}.

When equilibrium has been reached, the profile of j can be deduced from the T_e profile. The hollow T_e profiles result in hollow j profiles, with reversed magnetic shear out to ρ_{dep}, and a central safety factor (q_0) of 2.5–7.

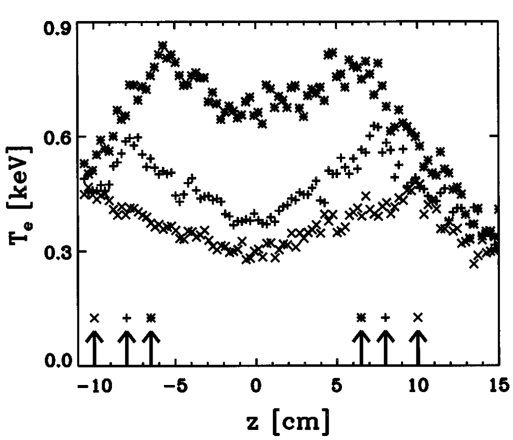

FIG. 3. T_e profiles during off-axis ECH, all with $n_e(0) \sim 4.0 \times 10^{19}$ m^{-3}, with different HFS absorption positions ρ_{dep}, marked by arrows [RTP discharges r19950622.053, (∗), r19950622.057 (+), and r19950622.065 (×)].

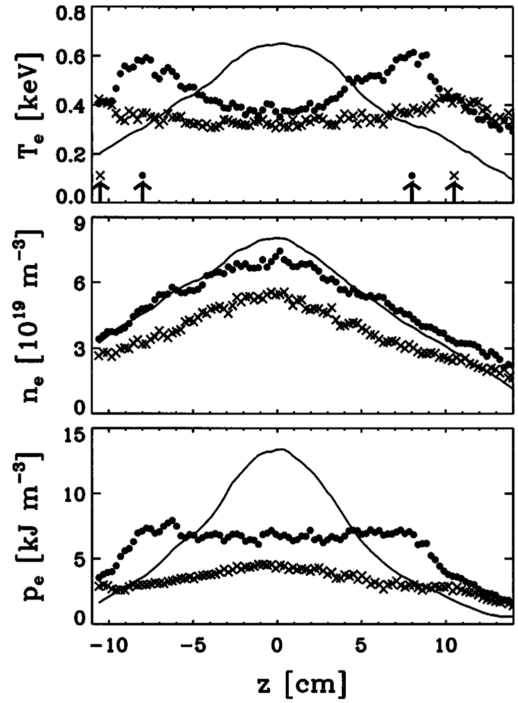

FIG. 4. T_e, n_e, and p_e profiles during off-axis ECH with LFS absorption [RTP discharges r19950620.021 (×) and r19950620.026 (•)]. The arrows mark ρ_{dep}. For comparison the profiles of a similar Ohmic discharge are shown (full line).

This is corroborated by polarimetry measurements, which show an increase of q_0 by a factor of $\sim$4 compared to the Ohmically heated plasma. Further confirmation comes from the sawtooth instability, which disappears within a few ms after the heating starts. The off-axis minimum of q ($q_{\min}$) varies between 1.5 and 3.5. Both q_0 and $q_{\min}$ increase with increasing ρ_{dep}. See Fig. 6 for a typical example.

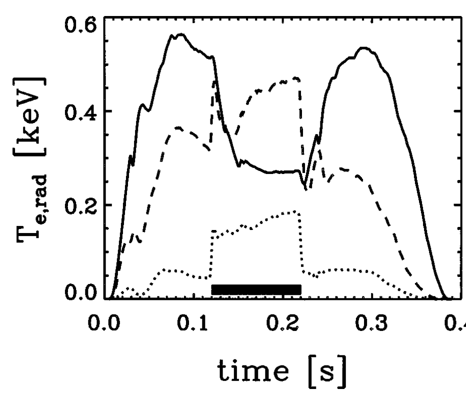

FIG. 5. Radiation temperature $T_{e,\text{rad}}$ for discharge r19950620.021 (see Fig. 4), measured by ECE at three different positions in the plasma: in the center (full line), near ρ_{dep} (dashed line), and outside ρ_{dep} (dotted line). ECH was applied from 120 to 220 ms, as indicated by the shaded area. Note the cooling in the center after the switch-on of the heating.

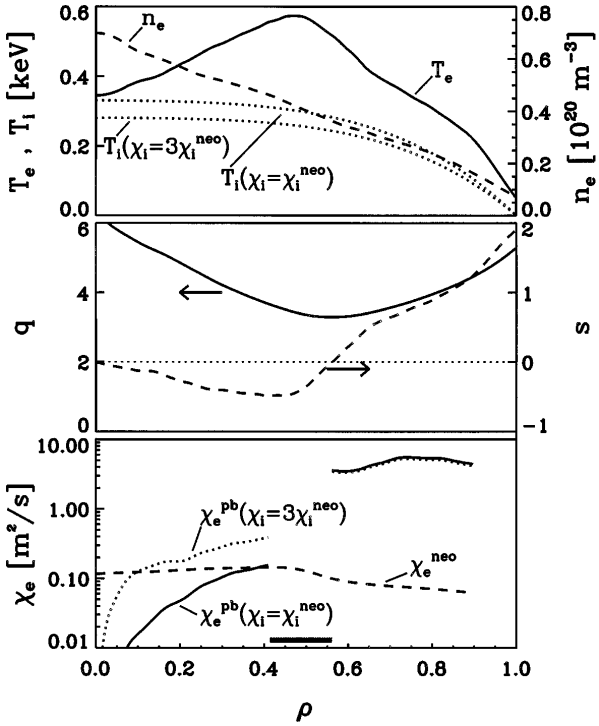

FIG. 6. LPB results for discharge r19950620.021. The upper box shows the smoothed TS profiles of $T_e(\rho)$ (full line) and $n_e(\rho)$ (dashed line), and the T_i profiles used in the analysis (see text, dotted lines). In the middle box q (full line) and shear parameter s (dotted line) are plotted, assuming full current penetration. The lower box shows χ_e^{pb}, under the two different assumptions for T_i (full and dotted line), plus the neoclassical prediction of χ_e (dashed line). The shaded area indicates the ECH power deposition zone.

The global electron energy confinement time ($\tau_{E,e}$), which in Ohmically heated medium to high density discharges in RTP is 3–5 ms, degrades to 1–3 ms with off-axis heating, and decreases with increasing $\rho_{\rm dep}$.

The effective electron thermal diffusivity $\chi_e^{pb} = q_e/n_e\nabla T_e$ (where q_e is the electron heat flux) was determined from a local electron power balance (LPB) analysis. Since no T_i measurements were available, two assumptions for the effective ion heat diffusivity (χ_i^{pb}) were considered: (i) $\chi_i^{pb} = \chi_i^{\rm neo}$ and (ii) $\chi_i^{pb} = 3\chi_i^{\rm neo}$, respectively ($\chi_i^{\rm neo}$ is the neoclassical ion thermal diffusivity). In the first case $T_i(0) \simeq 500$ eV in Ohmically heated plasmas, in agreement with earlier observations. Case (ii) gives an unrealistically low $T_i(0) \simeq 300$ eV in Ohmic plasmas, resulting in an upper estimate of χ_e^{pb} in the area with a hollow T_e profile. Radiation losses are low ($\simeq$10–20 kW, measured with bolometry) and are neglected in the present analysis. Full current adaptation has been assumed, which is justified since the profiles were taken about 4 current diffusion times after the switch-on of ECH. For the densities considered, ~95% of the ECH power is absorbed in the first pass. The power deposition zone has a FWHM of 3 cm (measured directly and calculated with ray tracing). In the analysis, 100% single pass absorption was assumed and all power is assumed to be deposited in a zone of 3 cm, which was omitted from the LPB analysis. Both assumptions give an upper estimate of the inward electron heat flux inside $\rho_{\rm dep}$, hence an upper estimate of χ_e^{pb}.

Spitzer resistivity has been assumed in the analysis, and the bootstrap current density ($j_{\rm boot}$) has been neglected. The off-axis heated discharges are only marginally in the banana regime in the region from $\rho \simeq \rho_{\rm dep}$ to $\rho \simeq 0.8$, and in the plateau regime elsewhere. The combined effect of the neoclassical correction to the resistivity and of $j_{\rm boot}$ is small, and leads to a slight enhancement of the central current density j_0.

Figure 6 shows χ_e^{pb} for a high density discharge with $\rho_{\rm dep} = 0.48$. The calculated χ_e^{pb} is close to or below neoclassical for $\rho < \rho_{\rm dep}$. Outside the power deposition zone $\chi_e^{pb} \geq 4$ m^2/s, the usual anomalous value for RTP.

For discharges just above the threshold density, the LPB analysis yields puzzling results. For such discharges, both assumptions on T_i cause p_{e-i} to be smaller than the residual ohmic power density (p_Ω) inside $\rho_{\rm dep}$, leading to a net outward electron heat flux, i.e., up the T_e gradient. Only the unrealistic assumption $T_i = 0$ would yield a net inward electron heat flux (see Fig. 7). This is a strong indication that off-diagonal elements in the transport matrix (the matrix relating the fluxes to the thermodynamical forces) are responsible for a significant

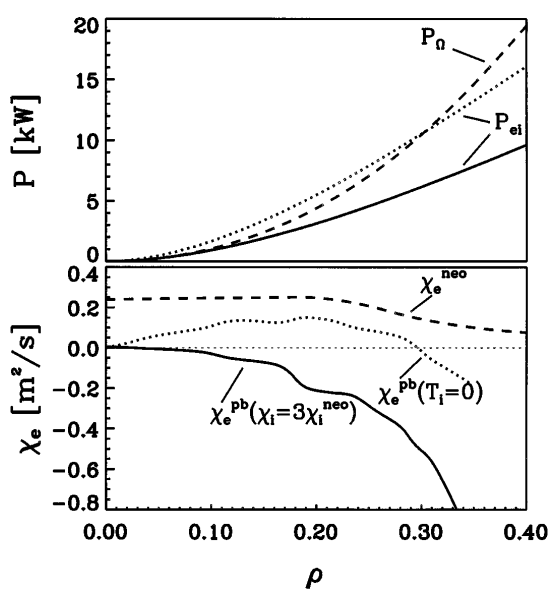

FIG. 7. LPB results for discharge r19950622.053 (see Fig. 3) for the area $\rho = 0$–0.4. The upper box shows P_Ω (the volume integrated p_Ω inside ρ, dashed line) and P_{e-i} (volume integrated p_{e-i} inside ρ) under two assumptions for T_i (see text, full and dotted lines). The lower box shows χ_e^{pb} (full and dotted lines), together with the neoclassical prediction of χ_e (dashed line). Only the unrealistic assumption $T_i = 0$ everywhere yields P_{e-i} larger than P_Ω, i.e., a positive χ_e^{pb}.

electron heat flux. First results of an experiment in which short heating pulses were applied in the center of the hollow T_e profile corroborate this view. The time constants associated with the induced rise and decay of $T_e(0)$ suggest that it is not χ_e itself that has changed, but that other, i.e., off-diagonal, terms are crucial in the electron heat flux. At this moment it is an open question which gradient drives this flux. Interestingly, during the evolution of the profiles, ∇T_e and the shear s go from negative to positive and back with different time constants, so that all possible combinations occur. A detailed, time dependent analysis may reveal the role of the current density distribution in driving a heat flux.

About the error on χ_e^{pb} inside ρ_{dep}, the following can be said. The systematic error on T_e and n_e from TS is small, $\leq 10\%$. Both profiles were smoothed for the LPB analysis, thus removing the effect of statistical errors, and causing the thus calculated χ_e^{pb} to be a radially averaged value. Regarding q_e, the assumptions on j, T_i, and the ECH power deposition were all made such that an upper estimate of χ_e^{pb} was obtained.

Transiently hollow T_e profiles have been observed in other tokamaks, for instance, in JET when off-axis ion cyclotron heating was applied after pellet injection [15]. There, the temporary hollowness was due to thermal inertia and the evolution of the $T_e \simeq T_i$ profile was proven to be diffusive.

There has been earlier evidence of reduced net heat transport in a region of reversed magnetic shear s, both theoretically [16] and experimentally. An example of the latter is the PEP mode in JET [17] which, however, is again transient in nature. Current drive can in principle sustain steady-state reversed shear, e.g., the lower hybrid enhanced performance regime in Tore Supra [18,19] and JET [20]. Recently, reversed shear configurations have drawn increasing interest as a possible scenario for a fusion reactor [21,22]. In the off-axis ECH discharges in RTP, reduced heat transport does not lead to improved global confinement, because no power is deposited in the region with reduced transport.

In contrast to observations in DIII-D [10], with off-axis ECH in RTP no peaking of T_e brought about by an inward heat pinch is observed. Still, as in DIII-D, evidence is found for a heat flow against ∇T_e. It should be noted, however, that the electron collisionality $\nu_e^* \simeq 1$ in high density discharges in RTP, whereas in DIII-D $\nu_e^* \ll 1$; this difference may provide an explanation for the different observations in DIII-D and RTP: the drift wave transport model that successfully simulated the DIII-D data [23] predicts an inward heat pinch only in the collisionless regime.

In this Letter we have shown that hollow T_e profiles have been sustained in RTP, thus breaking profile resilience. Extremely low net electron thermal transport is found in the region with inverted T_e gradient, in which also the magnetic shear is negative. The steady-state hollow T_e profile is a unique observation, achieved in RTP because of the very good localization of the 110 GHz 2nd harmonic X mode ECH, and the large ratio $P_{\mathrm{ECH}}/P_{\Omega} \simeq 5$.

The authors are indebted to the technical staff of RTP for the excellent machine operation and to F.C. Schüller for helpful discussions. This work was performed under the Euratom-FOM association agreement, with financial support from NWO and Euratom.

[1] B. Coppi, Comments Plasma Phys. Controlled Fusion **5**, 261 (1980).
[2] M. Murakami *et al.*, Plasma Phys. Controlled Fusion **28**, 17 (1986).
[3] F. Wagner *et al.*, Phys. Rev. Lett. **56**, 2187 (1986).
[4] G. Becker, Nucl. Fusion **31**, 663 (1991).
[5] F.C. Schüller *et al.*, in *Controlled Fusion and Plasma Physics, Proceedings of the 18th European Conference, Berlin, 1991* (European Physical Society, Geneva, 1991), Vol. 15C, Part IV, p. 185.
[6] B.B. Kadomtsev, Sov. J. Plasma Phys. **13**, 443 (1987).
[7] Yu.N. Dnestrovskij *et al.*, Nucl. Fusion **31**, 1877 (1991).
[8] B.B. Kadomtsev, Plasma Phys. Controlled Fusion **34**, 1931 (1992).
[9] J.B. Taylor, Phys. Fluids B **5**, 4378 (1993).
[10] C.C. Petty and T.C. Luce, Nucl. Fusion **34**, 121 (1994).
[11] A.A.M. Oomens *et al.*, in Proceedings of the 9th Joint Workshop on Electron Cyclotron Emission and Electron Cyclotron Resonance Heating, Borrego Springs, 1995 (to be published).
[12] C.J. Barth *et al.*, Rev. Sci. Instrum. **63**, 4947 (1992).
[13] C.C. Chu *et al.*, in *Controlled Fusion and Plasma Physics, Proceedings of the 21st European Conference, Montpellier, 1994* (European Physical Society, Geneva, 1994), Vol. 18B, Part III, p. 1248.
[14] J.H. Rommers *et al.*, in *Controlled Fusion and Plasma Physics, Proceedings of the 22th European Conference, Bournemouth, 1995* (European Physical Society, Geneva, 1995), Vol. 19C, Part III, p. 421.
[15] B. Balet *et al.*, Nucl. Fusion **34**, 1175 (1994).
[16] F. Romanelli and F. Zonca, Phys. Fluids B **5**, 4081 (1993).
[17] M. Hugon *et al.*, Nucl. Fusion **32**, 33 (1992).
[18] G.T. Hoang *et al.*, Nucl. Fusion **34**, 75 (1994).
[19] L. Guiziou *et al.*, in *Controlled Fusion and Plasma Physics, Proceedings of the 22th European Conference, Bournemouth, 1995* (European Physical Society, Geneva, 1995), Vol. 19C, Part I, p. 37.
[20] F.X. Söldner *et al.*, in Ref. [19], Part IV, p. 113.
[21] M.E. Mauel *et al.*, in Ref. [19], Part IV, p. 137.
[22] C. Kessel *et al.*, Phys. Rev. Lett. **72**, 1212 (1994).
[23] J. Weiland and H. Nordman, Phys. Fluids B **5**, 1669 (1993).